Supplementary Information for

Discovery of state-dependent inhibitors of the bacterial β-barrel assembly machine

Dawei Sun[1,*], Kelly M. Storek[2,*], Dimitry Tegunov[1,*], Ying Yang[3], Christopher P. Arthur[1,10], Matthew Johnson[1], John G. Quinn[4], Weijing Liu[5], Guanghui Han[5,11], Hany S. Girgis[2], Mary Kate Alexander[2], Austin K. Murchison[2], Stephanie Shriver[6], Christine Tam[6], Hiroshi Ijiri[7], Hiroko Inaba[7], Tatsuya Sano[7], Hayato Yanagida[7], Junichi Nishikawa[7], Christopher E. Heise[4,12], Wayne J. Fairbrother[8], Man-Wah Tan[2], Nicholas Skelton[3], Wendy Sandoval[5], Benjamin D. Sellers[3,13], Claudio Ciferri[1], Peter A. Smith[2,14], Patrick C. Reid[7], Christian N. Cunningham[9,15†], Steven T. Rutherford[2†], Jian Payandeh[1,2,16†]

[1]Genentech Inc., Structural Biology; South San Francisco, CA, United States.
[2]Genentech Inc., Infectious Diseases; South San Francisco, CA, United States.
[3]Genentech Inc., Discovery Chemistry; South San Francisco, CA, United States.
[4]Genentech Inc., Biochemical and Cellular Pharmacology; South San Francisco, CA, United States.
[5]Genentech Inc., Microchemistry, Proteomics and Lipidomics; South San Francisco, CA, United States.
[6]Genentech Inc., BioMolecular Resources; South San Francisco, CA, United States.
[7]PeptiDream Inc., Kawasaki, Kanagawa, Japan.
[8]Genentech Inc., Early Discovery Biochemistry; South San Francisco, CA, United States.
[9]Genentech Inc., Peptide Therapeutics; South San Francisco, CA, United States.
[10]Current: Altos Labs; Redwood City, CA, United States.
[11]Current: PTM Bio; Alameda, CA, United States.
[12]Current: Septerna; South San Francisco, CA, United States.
[13]Current: Vilya; South San Francisco, CA, United States.
[14]Current: Revagenix; San Mateo, CA, United States.
[15]Current: PeptiDream; Kawasaki, Japan.
[16]Current: Exelixis; Alameda, CA, United States.

*These authors contributed equally to this work: D.S., K.M.S., and D.T.

†Corresponding authors. Email: C-cunningham@peptidream.com (C.C.); rutherford.steven@gene.com (S.T.R.); jpayandeh@exelixis.com (J.P.)

Contents **pages**

Supplementary Figure 1

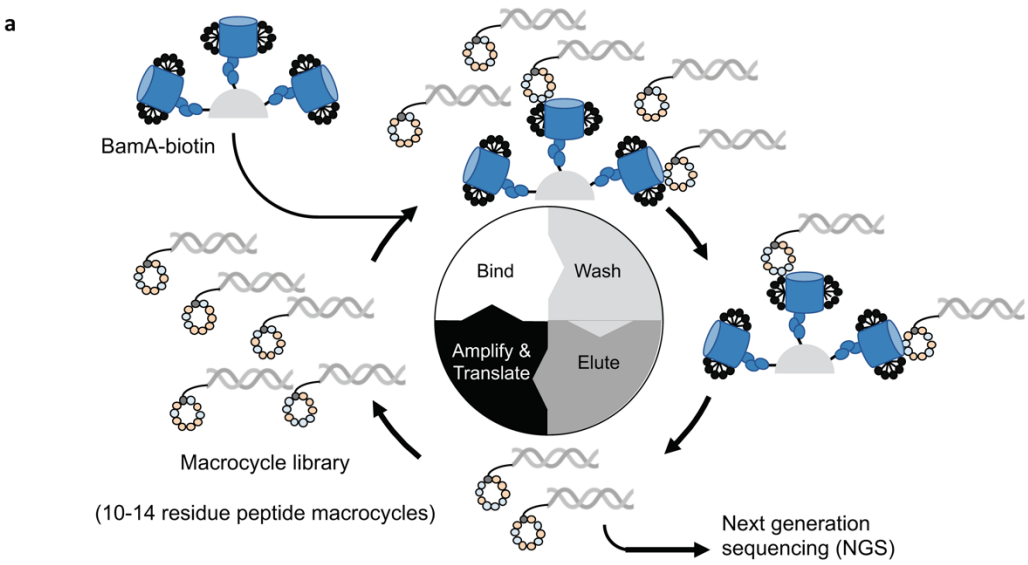

b

Selections performed against BamA in octylglucoside

Macrocycle	Sequence	Frequency	ELISA	MIC (μM)
PTB1	FVWHGSRmFHRHC	63.04	+	50
114	FYHGHmFHLWC	11.34	+	>100
115	FYHNHmFHLWC	1.31	+	>100
116	FRmFmAVYWWYDmFC	1.28	+	>100
117	FPHmFVmFNWVHVHYC	1.14	+	>100
118	FWGHYPDmFYmFVHC	1.06	+	>100
119	FRGYVmGVYWYWC	1.03	+	>100
120	FHYNmFRmAmFNVSWC	0.74	+	>100
122	FGmFmAVYWWYDLC	0.73	+	>100
121	FRGYVmGVYWYDC	0.73	+	>100
123	FRmFmAVYWWYDLC	0.67	+	>100
124	FRmFmAVYWWYSmFC	0.61	+	>100
125	FVWHGSRmFHLWC	0.36	+	>100
127	FLHYHRSVLHDmFC	0.34	+	>100

Selections performed against BAM in octylglucoside

Macrocycle	Sequence	Frequency	ELISA	MIC (μM)
PTB2	FGTIHKRRFRYWFC	0.08	+	4
94	FSIWYFHPGVVIVC	73.72	+	>100
95	FSYVRKSIVRKRFC	6.76	+	>100
96	FSVHRGEIIRKSFC	2.67	+	>100
99	FSVTRGFIIRKWFC	0.67	+	>100
109	FSVHRGDIIRKSFC	0.20	+	>100
111	FHRIRRLAIYYWYC	0.15	+	>100
154	FSYVSGRIIRKVFC	0.11	+	>100
155	FLYYNRSFLWFSWC	0.09	+	>100

c

Macrocycle	PTB1		119		PTB2	
WT MIC activity	+		-		+	
Protein	BamA	BAM	BamA	BAM	BamA	BAM

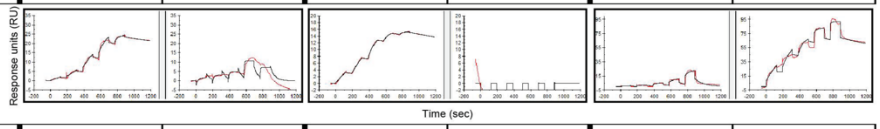

k_a (1/Ms)	2.027E+5	3.658E+6	4.467E+5	6.980E+4	6680	6.263E+4
k_d (1/s)	3.563E-4	0.01976	3.352E-4	0.2793	0.008906	4.310E-4
K_D (M)	1.177E-9	5.403E-9	7.502E-10	4.002E-6	1.333E-6	6.881E-0

Supplementary Figure 1. Discovery of macrocyclic peptides targeting BamA.
a. Schematic of the mRNA display macrocycle discovery approach. See methods for details. BamA-biotin (with POTRA3-5 domains) is shown in blue and NGS indicates next generation sequencing.
b. Exemplar macrocycles from mRNA display selections against BamA (with POTRA3-5 domains) recombinant protein and purified BAM complex with NGS frequency and MIC activity against *E. coli* ATCC 25922 done in high-throughput during the discovery process are indicated.
c. SPR sensorgrams of indicated macrocycles binding to BamA or the BAM complex in octyl-glucoside detergent conditions at 25°C *in vitro*. Data traces (red) and 1:1 binding modeling (black), which was used to derive indicated kinetic constants, are shown. Peptide 119 is shown as an example of a macrocycle that binds but lacks wild-type MIC activity. These binding observations were used as single experiments to choose macrocycles in our discovery selection funnel and not to analyze the binding kinetics and are thus shown only to illustrate the extent of observed binding.

Supplementary Figure 2

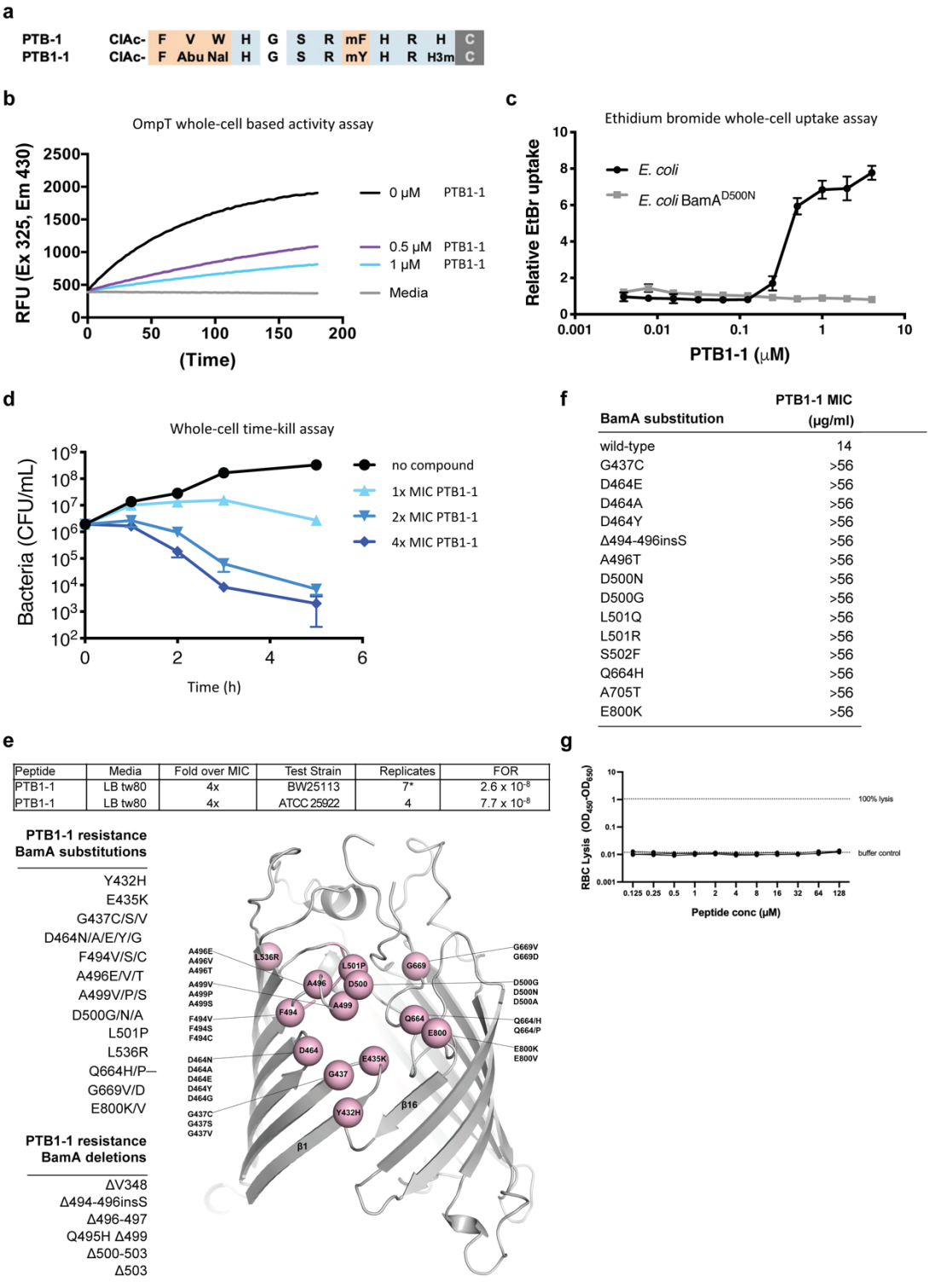

Supplementary Figure 2. Characterization of PTB1-1.
a. Schematic of the 12-amino acid sequences of the BamA-binding macrocycles PTB1 and PTB1-1.
b. A fluorogenic OmpT peptide substrate was used to assay BAM activity in live *E. coli* BW25113 cells in the absence (black) or presence of PTB1-1 (0.5 μM in purple, 1 μM in cyan). A media control is shown in gray. The means of quadruplicate technical replicates is plotted and is a representative of two independent experiments. Data used to generate the plot are provided in Supplementary Data S2B in the Source Data.
c. An ethidium bromide uptake assay performed against *E. coli* BW25113 was used to monitor outer membrane permeability in the presence of increasing concentrations of the BamA-binding macrocycle PTB1-1. Assay was performed with wild-type (black circles) and a PTB1-1-resistant mutant strain (D500N) (gray squares). The means and standard deviations of quadruplicate technical replicates is plotted and is a representative of two independent experiments. Data used to generate the plot are provided in Supplementary Data S2C in the Source Data.
d. A time-kill assay performed against wild-type *E. coli* BW25113 was performed in the absence (black) or presence of PTB1-1 (1x MIC in light blue, 2x MIC in blue, and 4x MIC in dark blue). The average and standard deviation of CFU/mL at times after addition of the macrocycles is plotted. The means and standard deviations of triplicate technical replicates (n=3) is plotted. Data used to generate the plot are provided in Supplementary Data S2D in the Source Data.
e. Frequencies of resistance calculated from selections performed with PTB1-1 against wild-type *E. coli* BW25113 and wild-type *E. coli* ATCC 25922 were determined at 4x MIC. The position of each PTB1-1 resistant substitution is highlighted on the closed lateral gate structure of PTB1-1-BamA as pink spheres, with the macrocycle removed for clarity.
f. Minimal Inhibitory Concentrations (MICs) of PTB1-1 against wild-type *E. coli* BW25113 and mutants selected for resistance to PTB1-1.
g. Red blood cell (RBC) lysis assay with PTB1-1. Lysis was measured after 4 hours of incubation with indicated concentrations of PTB1-1, 0.5% Triton X-100 (set to 100% lysis), or buffer (set to 0% lysis). Assay was performed in quadruplicate and all four replicates are plotted. Data used to generate the plot are provided in Supplementary Data S2G in the Source Data.

Supplementary Figure 3

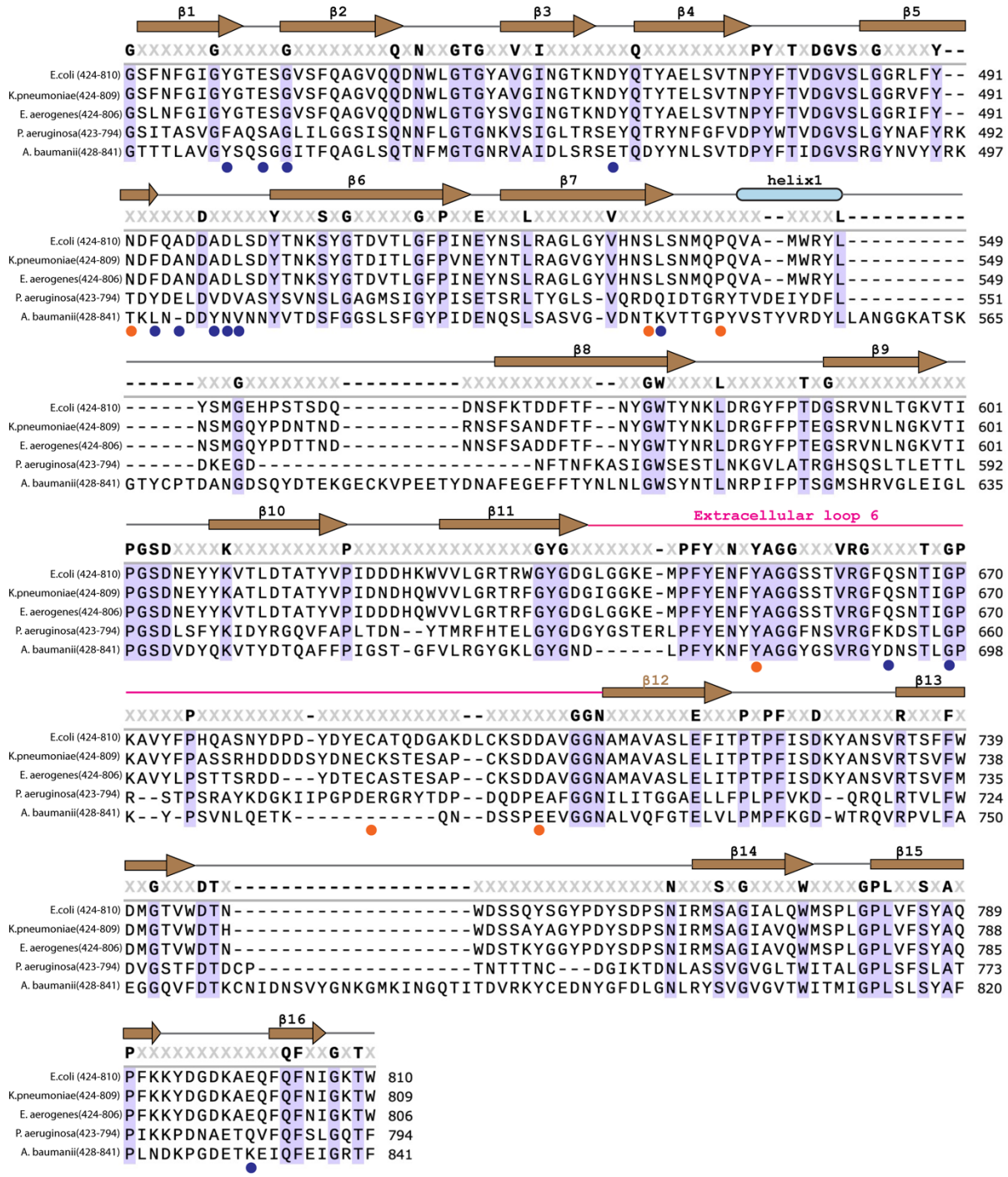

Supplementary Figure 3. BamA β-barrel sequence alignment.
Alignment of the BamA β-barrel sequences from *E. coli* (residues 424-810), *K. pneumoniae* (residues 424-809), *E. aerogenes* (residues 424-806), *P. aeruginosa* (residues 423-794), and *A. baumannii* (residues 428-841). Secondary structural features (as observed in PTB1-1-BAM structure) are indicated above the sequence. Residues with a consensus score >70% are highlighted in purple and positions where substitutions lead to PTB1-1 and PTB2-1 resistance are noted with a blue and orange dot, respectively. Extracellular loop 6 is colored in magenta. Sequences were aligned using SnapGene (version 6.2.1).

Supplementary Figure 4

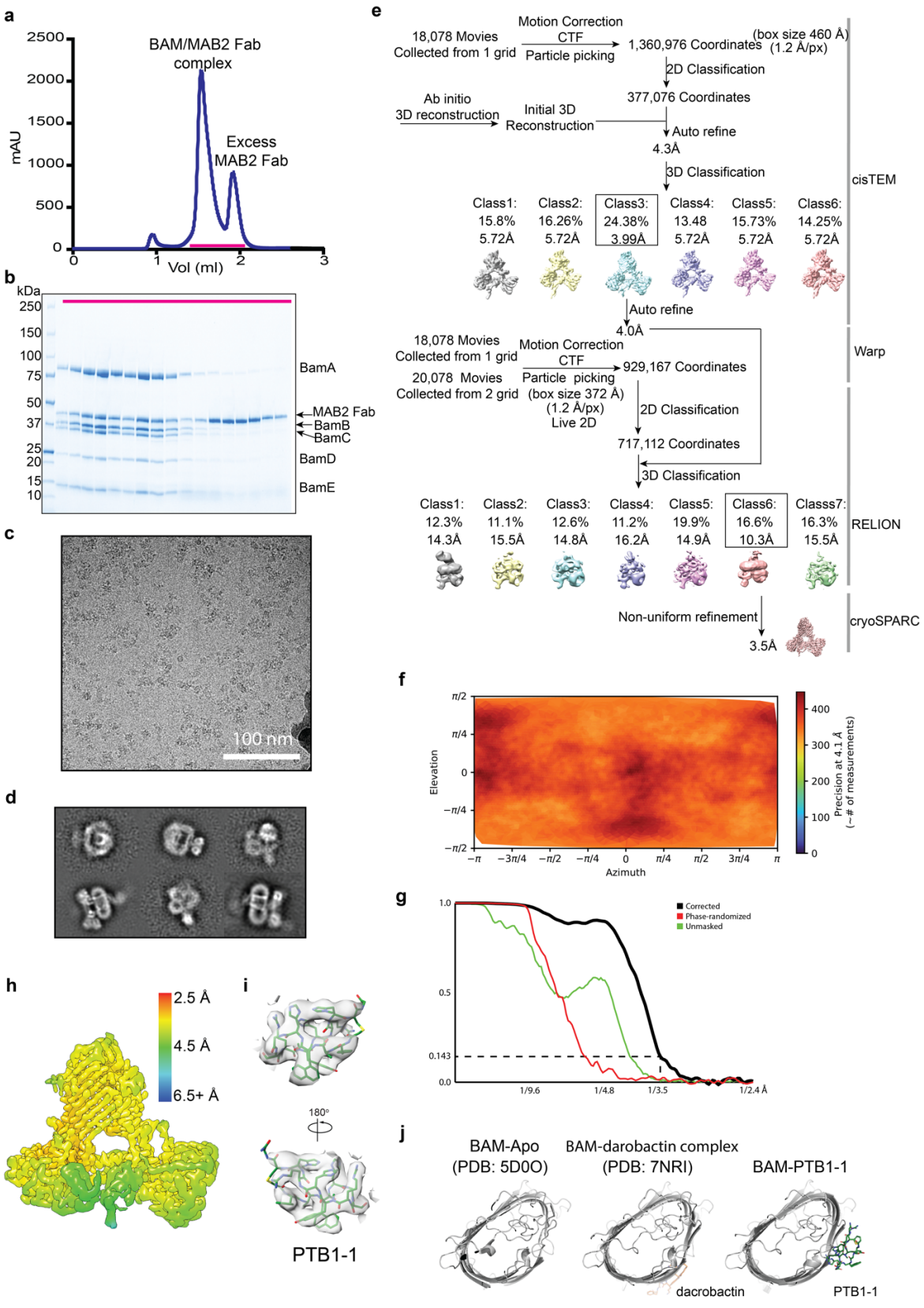

Supplementary Figure 4. Cryo-EM sample, imaging, and structure determination of the PTB1-1-BAM-MAB2 Fab complex.
a. Size exclusion chromatography (SEC) profile of the BAM-MAB2 Fab complex which was purified in DDM.
b. SDS-PAGE analysis of the SEC of the BAM-MAB2 Fab complex. Full uncropped gel image is included in Supplementary Data S4B in the Source Data.
c. Representative micrograph of the PTB1-1-BAM-MAB2 Fab complex sample.
d. Representative 2D-class averages from cisTEM containing PTB1-1-BAM-MAB2 Fab complex (particle box size: 372 Å).
e. Data processing workflow.
f. Angular distribution calculated in cryoSPARC for particle projections.
g. Gold-standard FSC curves from cryoSPARC and the reported resolution at FSC=0.143 shown by the horizontal line.
h. Isosurface rendering of the 3D map with surface coloring according to the local resolution estimated by windowed FSCs.
i. Cryo-EM map of PTB1-1.
j. BamA (top-down views) structure in the absence of inhibitor (*left*: BAM-apo, PDB 5D0O[1]) compared to BamA in the presence of inhibitors (*middle*: BAM-darobactin complex, PDB 7NRI[2]; and *right*: PTB1-1-BAM).

Supplementary Figure 5

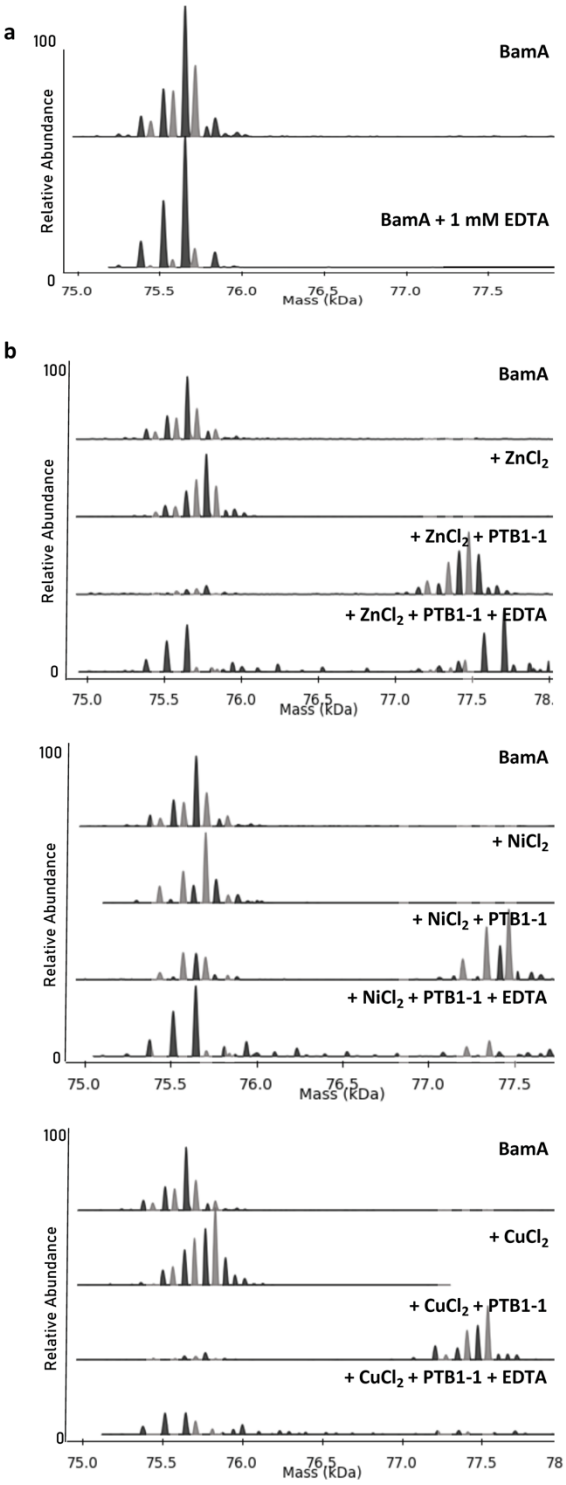

c

PTB1-1 variant	seqeunce	MIC (μM)
PTB1-1	ClAc- F Abu Nal1 H G S R mY H R H3M C G NH2	0.2
PTB1-1.A1	ClAc- **A** Abu Nal1 H G S R mY H R H3M C G NH2	12.5
PTB1-1.A2	ClAc- F **A** Nal1 H G S R mY H R H3M C G NH2	1.56
PTB1-1.A3	ClAc- F Abu **A** H G S R mY H R H3M C G NH2	>100
PTB1-1.A4	ClAc- F Abu Nal1 **A** G S R mY H R H3M C G NH2	>100
PTB1-1.A5	ClAc- F Abu Nal1 H **A** S R mY H R H3M C G NH2	3.125
PTB1-1.A6	ClAc- F Abu Nal1 H G **A** R mY H R H3M C G NH2	12.5
PTB1-1.A7	ClAc- F Abu Nal1 H G S **A** mF H R H3M C G NH2	>100
PTB1-1.A8	ClAc- F Abu Nal1 H G S R **A** H R H3M C G NH2	>100
PTB1-1.mA8	ClAc- F Abu Nal1 H G S R mA H R H3M C G NH2	>100
PTB1-1.A9	ClAc- F Abu Nal1 H G S R mY **A** R H3M C G NH2	>100
PTB1-1.A10	ClAc- F Abu Nal1 H G S R mY H **A** H3M C G NH2	50
PTB1-1.A11	ClAc- F Abu Nal1 H G S R mY H R **A** C G NH2	>100

Supplementary Figure 5. Native mass spectrometry analysis of the PTB1-1-BamA complex and PTB1-1 mutational scanning analysis.

a. Mass spectrum of purified BamA in detergent with or without 1 mM EDTA. Spectra are representative of n>3 experiments.

b. Mass spectrum of purified BamA in detergent in the presence or absence of 1 μM PTB1-1 and 2 μM $ZnCl_2$, $NiCl_2$ or $CuCl_2$, and/or 1 mM EDTA. Experiments were performed at 1, 2, 5, and 10 μM of each metal ion and representatives of n>3 experiments at 2 μM are shown.

c. Macrocycle sequences and MIC activity against *E. coli* ATCC 25922 indicated.

Supplementary Figure 6

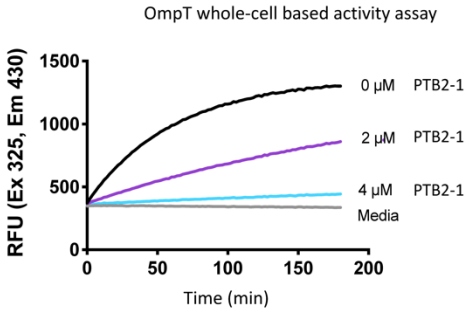

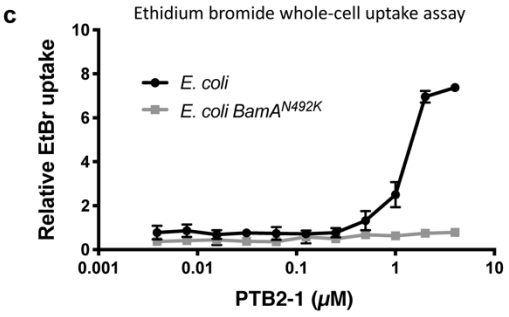

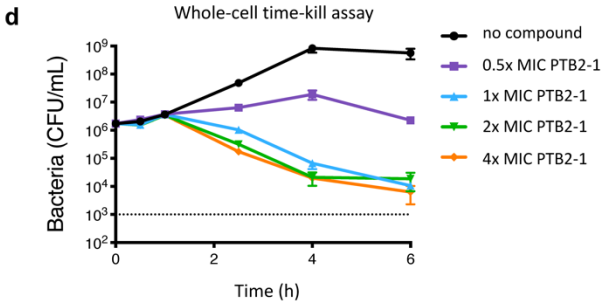

f

BamA substitutions	Macrocycle used in selection	PTB2 MIC (μg/mL)	PTB2-1 MIC (μg/mL)
Wild-type	-	4	8
G427C	PTB1	4	1
D500N	PTB1	8	4
Q664H	PTB1	8	16
E800K	PTB1	8	8
N492K	PTB2	32	>64
P541L	PTB2	32	128
C690W	PTB2	32	128
S537P	PTB2	16	>128
Y653D	PTB2	16	>128
C690Y	PTB2	16	>128

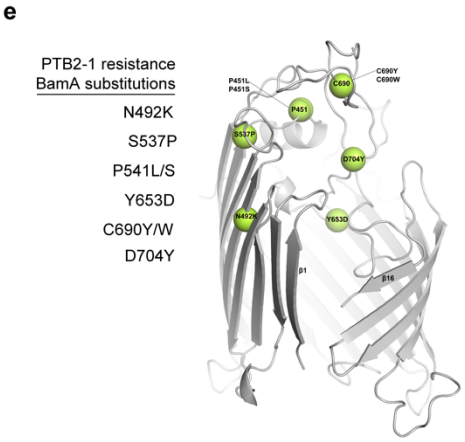

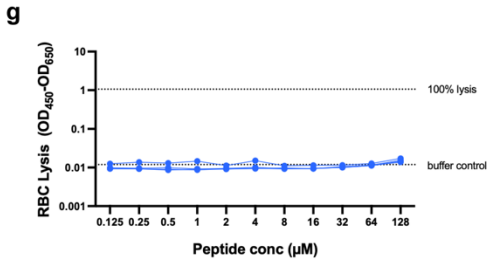

Supplementary Figure 6. Characterization of PTB2-1.
a. Schematic of the 14-amino acid sequences of the BamA-binding macrocycles PTB2 and PTB2-1.
b. A fluorogenic OmpT peptide substrate was used to assay BAM activity in live *E. coli* BW25113 cells in the absence (black) or presence of PTB2-1 (2 μM in purple, 4 μM in cyan). A media control is shown in gray. The means of quadruplicate technical replicates is plotted and is a representative of two independent experiments. Data used to generate the plot are provided in Supplementary Data S6B in the Source Data.
c. An ethidium bromide uptake assay performed against *E. coli* BW25113 was used to monitor outer membrane permeability in the presence of increasing concentrations of the BamA-binding macrocycle PTB2-1. Assay was performed with wild-type (black circles) and a PTB2-1-resistant mutant strain (N492K) (gray squares). The means and standard deviations of quadruplicate technical replicates is plotted and is a representative of two independent experiments. Data used to generate the plot are provided in Supplementary Data S6C in the Source Data.
d. A time-kill assay performed against wild-type *E. coli* BW25113 was performed in the absence (black) or presence of PTB2-1 (0.5x MIC in purple, 1x MIC in light blue, 2x MIC in green, and 4x MIC in orange). The means and standard deviation of CFU/mL from technical triplicates (n=3) at times after addition of the macrocycles are plotted. The horizontal dashed line is the limit of detection for these experiments. Data used to generate the plot are provided in Supplementary Data S6D in the Source Data.
e. The position of each PTB2-1 resistant substitution highlighted on the open lateral gate cryo-EM structure of PTB2-BAM as green spheres, with the macrocycle removed for clarity.
f. Minimal Inhibitory Concentrations (MICs) of PTB1 and PTB2-1 against wild-type *E. coli* BW25113 and mutants selected for resistance to PTB1 and PTB2-1.
g. Red blood cell (RBC) lysis assay with PTB2-1. Lysis was measured after 4 hours of incubation with indicated concentrations of PTB1-1, 0.5% Triton X-100 (set to 100% lysis), or buffer (set to 0% lysis). Assay was performed in quadruplicate and all four replicates are plotted (and highly overlapping). Data used to generate the plot are provided in Supplementary Data S6G in the Source Data.

Supplementary Figure 7

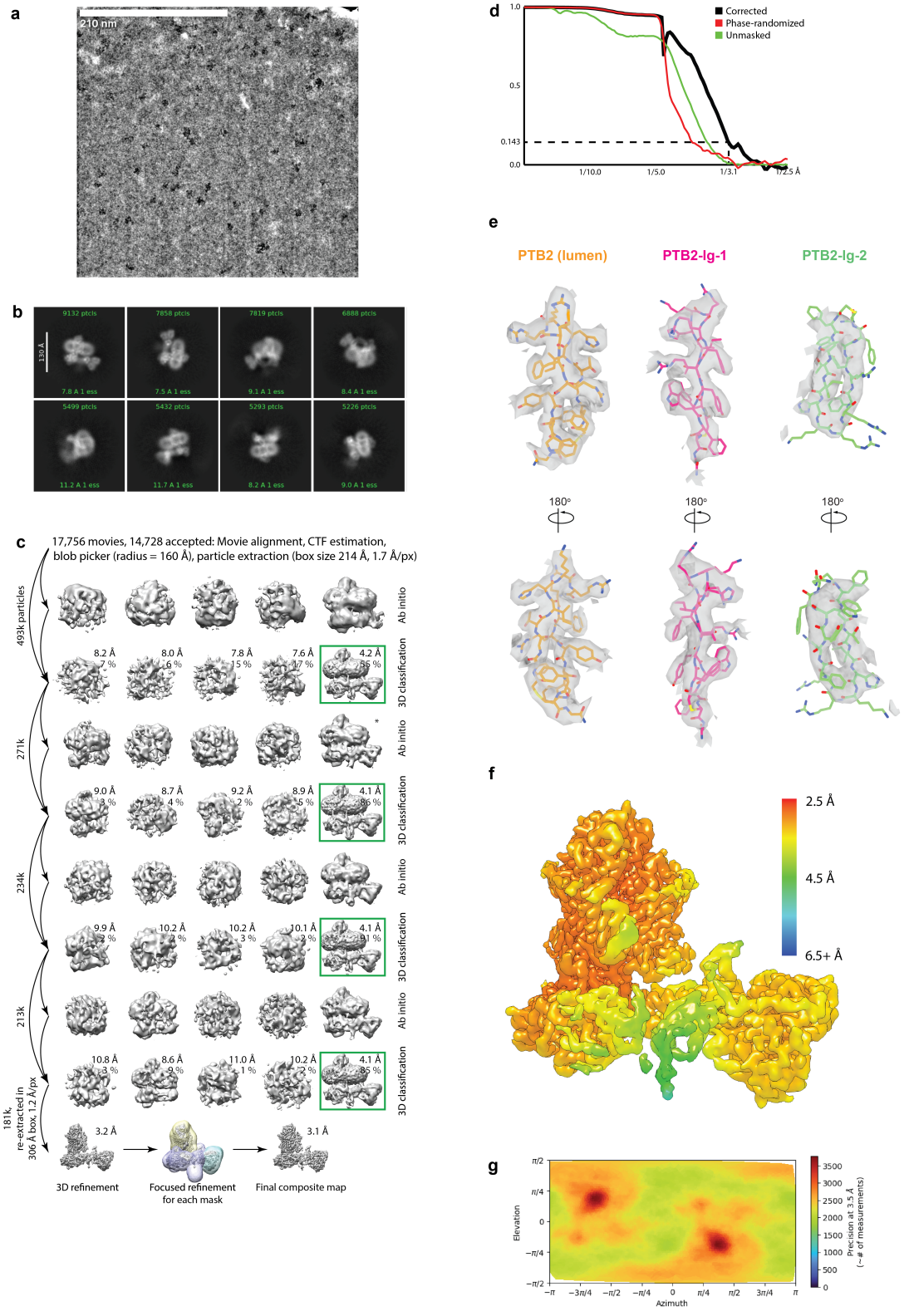

Supplementary Figure 7. Cryo-EM imaging and structure determination of the PTB2-BAM-DDM complex.
a. Representative micrograph from the data set showing the particle distribution.
b. Representative 2D classes from cryoSPARC containing the PTB2-BAM-DDM complex (particle box size: 318 Å).
c. Data processing workflow. CryoSPARC was used for all steps. Particles were sorted over 4 iterations of generating *ab initio* references and using them for supervised 3D classification. Green frames mark 3D classes whose particles were selected for the next processing step. * marks an *ab initio* reference also used for supervised 3D classification of PTB2-SMA data.
d. Gold-standard, phase randomization-corrected FSC curves from cryoSPARC and the reported resolution at FSC=0.143 (dashed line).
e. 3D map overlay for PTB2-lumen, PTB2-lg-1 and PTB2-lg-2.
f. Isosurface rendering of the 3D map with surface coloring according to the local resolution estimated by windowed FSC.
g. Direction-dependent Fourier-space coverage calculated in cryoSPARC, showing how many particle images contributed to the reconstruction in each direction.

Supplementary Figure 8

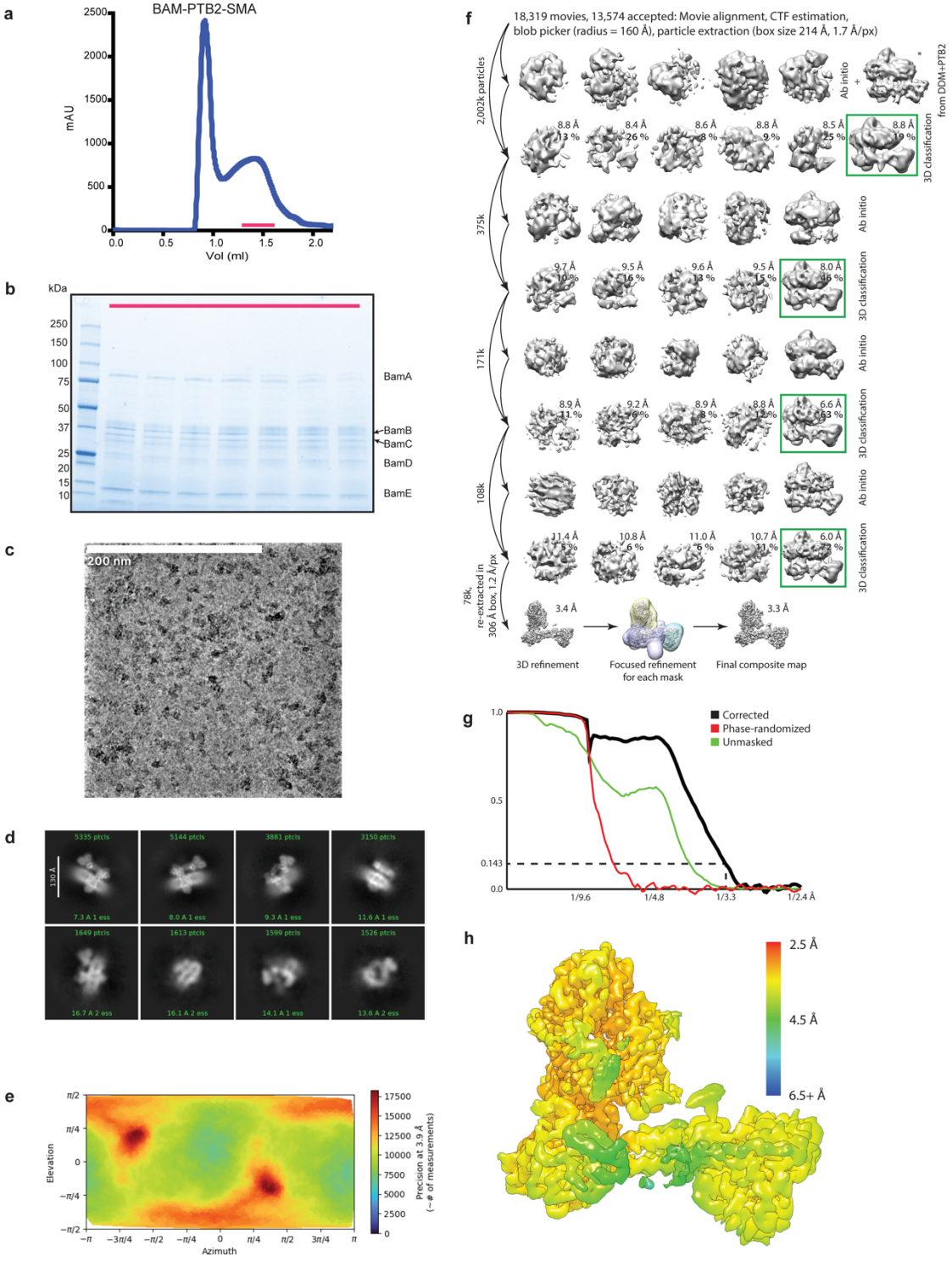

Supplementary Figure 8. Cryo-EM imaging and structure determination of the PTB2-BAM-SMA complex.
a. SEC profile of the PTB2-BAM-SMA complex.
b. SDS-PAGE analysis of the SEC of the PTB2-BAM-SMA complex. Full uncropped gel image is included in Supplementary Data S8B in the Source Data.
c. Representative micrograph from the data set; white circles mark final particle selection.
d. Representative 2D classes from cryoSPARC containing the PTB2-BAM-SMA complex (particle box size: 280 Å).
e. Direction-dependent Fourier-space coverage calculated in cryoSPARC, showing how many particle images contributed to the reconstruction in each direction.
f. Data processing workflow. CryoSPARC was used for all steps. Particles were sorted over 4 iterations of generating *ab initio* references and using them for supervised 3D classification. Green frames mark 3D classes whose particles were selected for the next processing step. * marks a reference borrowed from PTB2-DDM data processing.
g. Gold-standard, phase randomization-corrected FSC curves from cryoSPARC and the reported resolution at FSC = 0.143 (dashed line).
h. Isosurface rendering of the 3D map with surface coloring according to the local resolution estimated by windowed FSC.

Supplementary Figure 9

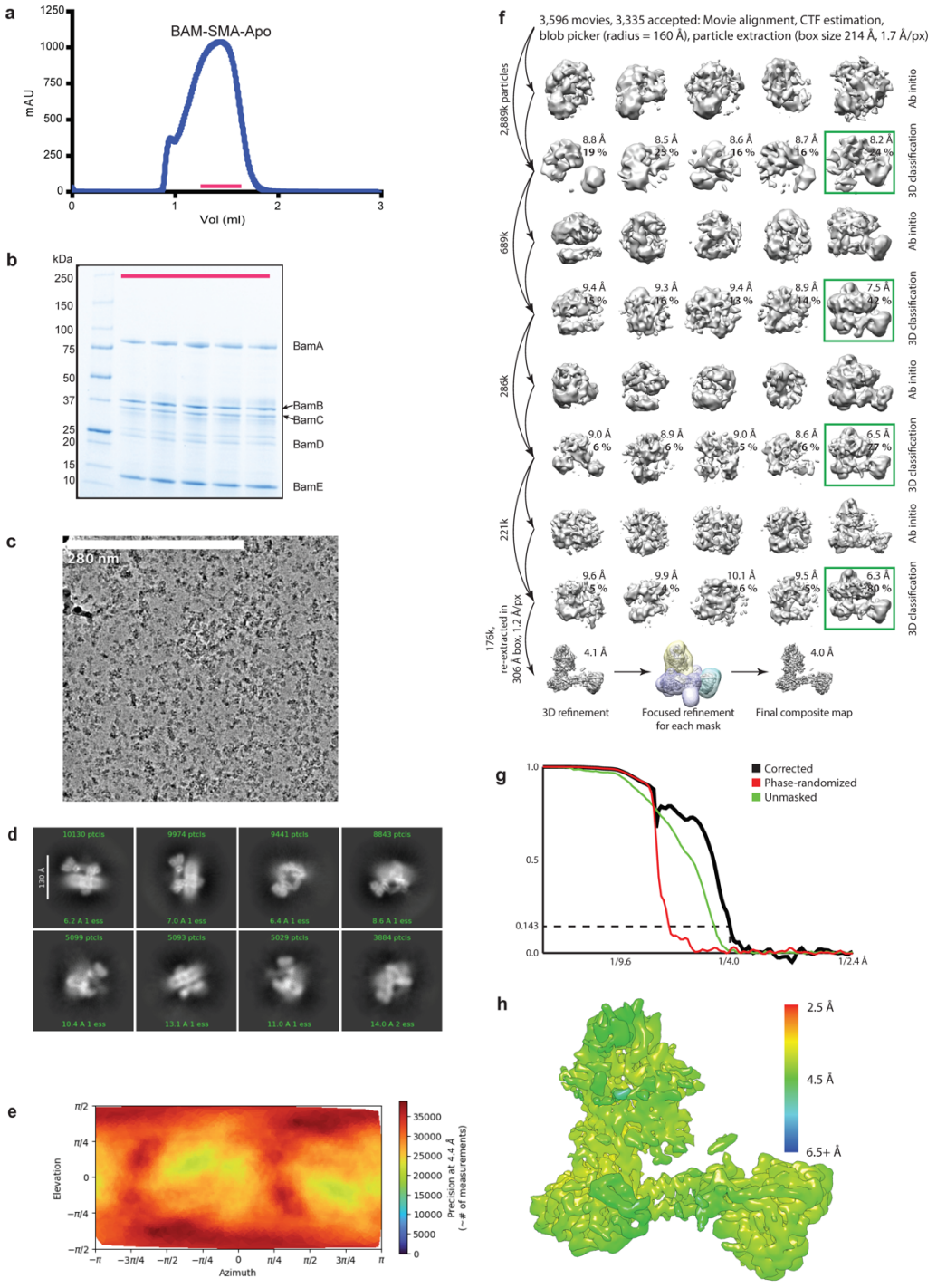

Supplementary Figure 9. Cryo-EM imaging and structure determination of the apo BAM-SMA.
a. SEC profile of the apo BAM-SMA complex.
b. SDS-PAGE analysis of the SEC of the apo BAM-SMA complex. Full uncropped gel image is included in Supplementary Data S9B in the Source Data.
c. Representative micrograph from the data set; white circles mark final particle selection.
d. Representative 2D classes from cryoSPARC containing the apo BAM-SMA complex (particle box size: 280 Å).
e. Direction-dependent Fourier-space coverage calculated in cryoSPARC, showing how many particle images contributed to the reconstruction in each direction.
f. Data processing workflow. CryoSPARC was used for all steps. Particles were sorted over 4 iterations of generating *ab initio* references and using them for supervised 3D classification. Green frames mark 3D classes selected for the next processing step.
g. Gold-standard, phase randomization-corrected FSC curve from cryoSPARC and the reported resolution at FSC=0.143 (dashed line).
h. Isosurface rendering of the 3D map with surface coloring according to the local resolution estimated by windowed FSC.

Supplementary Figure 10

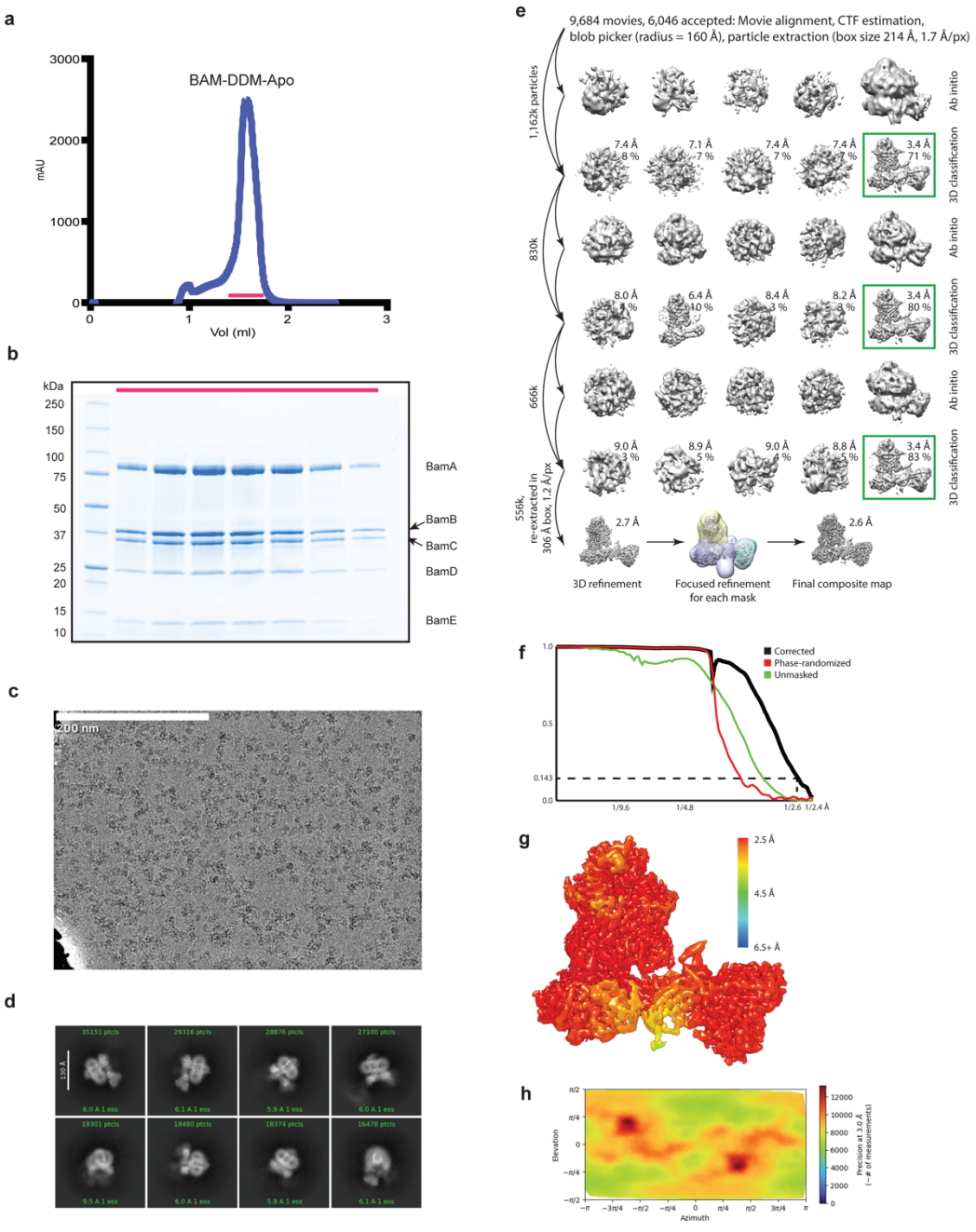

Supplementary Figure 10. Cryo-EM imaging and structure determination of the apo BAM-DDM.
a. SEC profile of the apo BAM-DDM complex.
b. SDS-PAGE analysis of the SEC of the apo BAM-DDM complex. Full uncropped gel image is included in Supplementary Data S10B in the Source Data.
c. Representative micrograph from the data set showing the particle distribution.
d. Representative 2D classes from cryoSPARC containing the apo BAM-DDM complex (particle box size: 307 Å).
e. Data processing workflow. CryoSPARC was used for all steps. Particles were sorted over 3 iterations of generating *ab initio* references and using them for supervised 3D classification. Green frames mark 3D classes selected for the next processing step.
f. Gold-standard, phase randomization-corrected FSC curve from cryoSPARC and the reported resolution at FSC=0.143 (dashed line).
g. Isosurface rendering of the 3D map with surface coloring according to the local resolution estimated by windowed FSC.
h. Direction-dependent Fourier-space coverage calculated in cryoSPARC, showing how many particle images contributed to the reconstruction in each direction.

Supplementary Figure 11

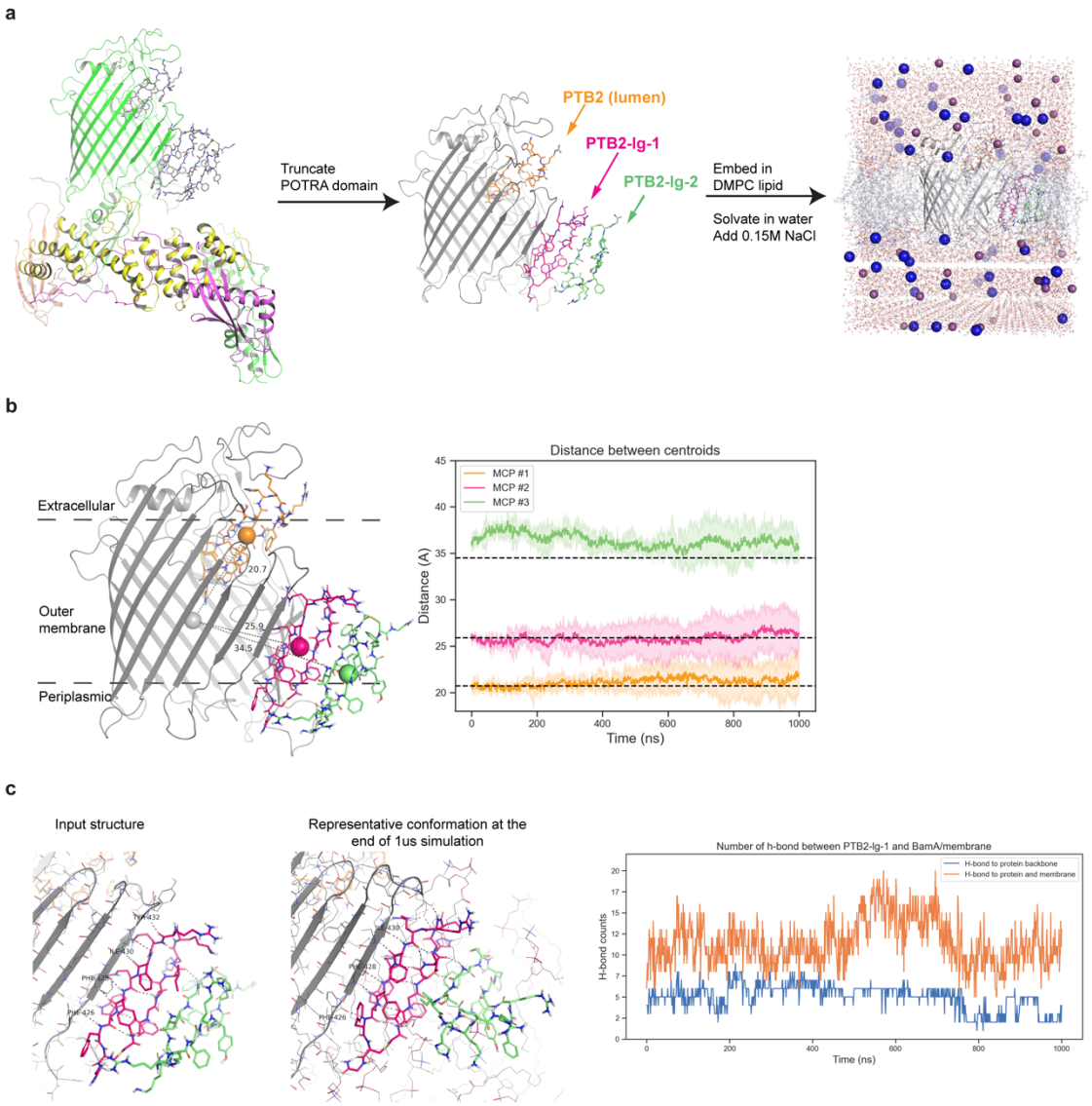

Supplementary Figure 11. Molecular dynamics simulations of PTB2-BamA complex
a. System setup for molecular dynamics simulations.
b. Stability of BamA and PTB2 during molecular dynamics simulations. Distance between the centroids of BamA and PTB2 remains stable during the 1 μs molecular dynamics simulation.
c. Hydrogen bond interactions between BamA and lateral gate PTB2 molecules during molecular dynamics simulations. The number of hydrogen bonds between PTB2-lg-1 and BamA backbone fluctuates but remains stable around three, while to BamA side chains and the membrane the number varies more around ten. Note that input and output files from molecular dynamics simulations are provided in Supplementary Data 3E in the Source Data.

Supplementary Figure 12

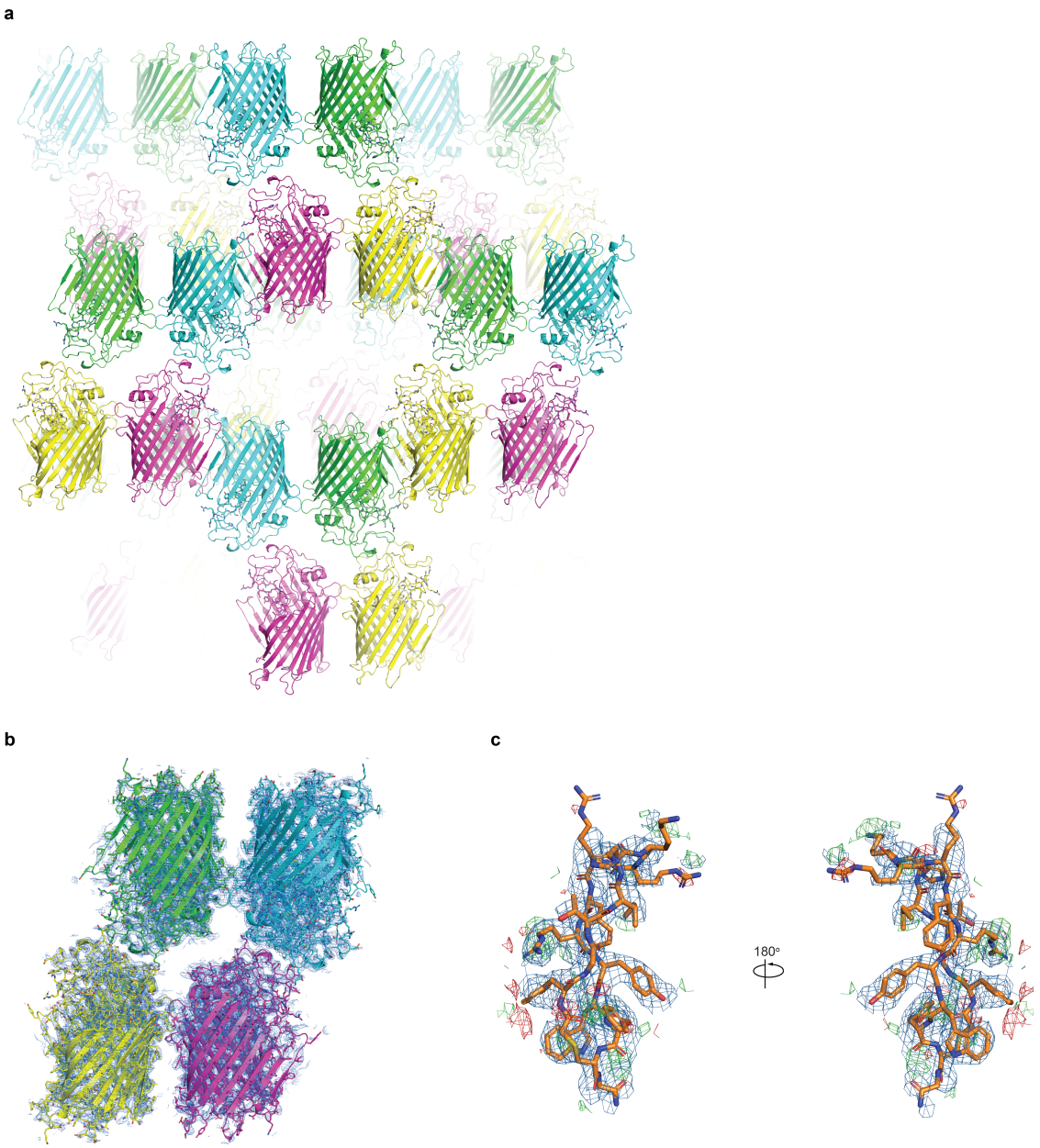

Supplementary Figure 12. Crystal structure of PTB2-BamA complex.
a. Lattice packing of the PTB2-BamA complex with pairs of BamA molecules interacting inverted relative to each outer.
b. Overall structure of the asymmetric unit content contains four PTB2-BamA complexes which were filled in a 2Fo-Fc map contoured at σ = 1.
c. 2Fo-Fc map (blue, contoured at 1 σ) and Fo-Fc map (green/red, contoured at ± 3 σ) for PTB2.

Supplementary Figure 13

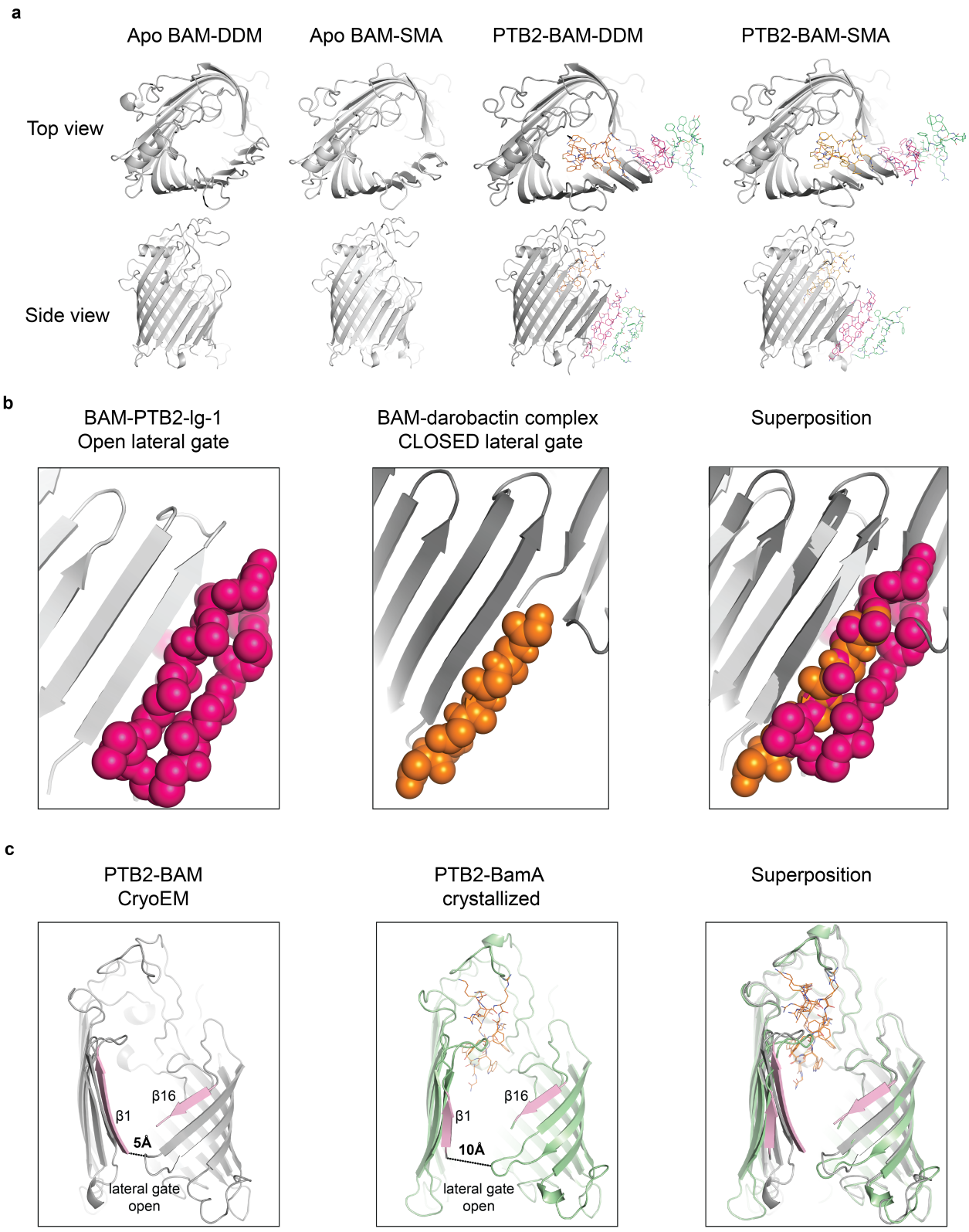

Supplementary Figure 13. Comparison of PTB2-BAM complex

a. Comparison of BamA β-barrel conformation in Apo and PTB2 bound states. Apo and PTB2 bound structures are displayed with both top view and side view.

b. Comparison between PTB2-BAM complex and BamA-darobactin structure. PTB2-lg-1 backbone (pink) and darobactin backbone (orange) in the closed lateral gate of BAM (PDB: 7NRI[2]) are shown sphere representation for simplicity.

c. Comparison of the open lateral gate of BamA β-barrel between PTB2-BAM cryo-EM structure (gray) and PTB2-BamA crystal structure (green). BamA β1 and A β16 of the lateral gate are colored in light pink. The distance is measured between S425 and L789 (closeted with S425 in the lateral gate) in both PTB2-BAM cryo-EM and PTB2-BamA crystal structure.

Supplementary Figure 14

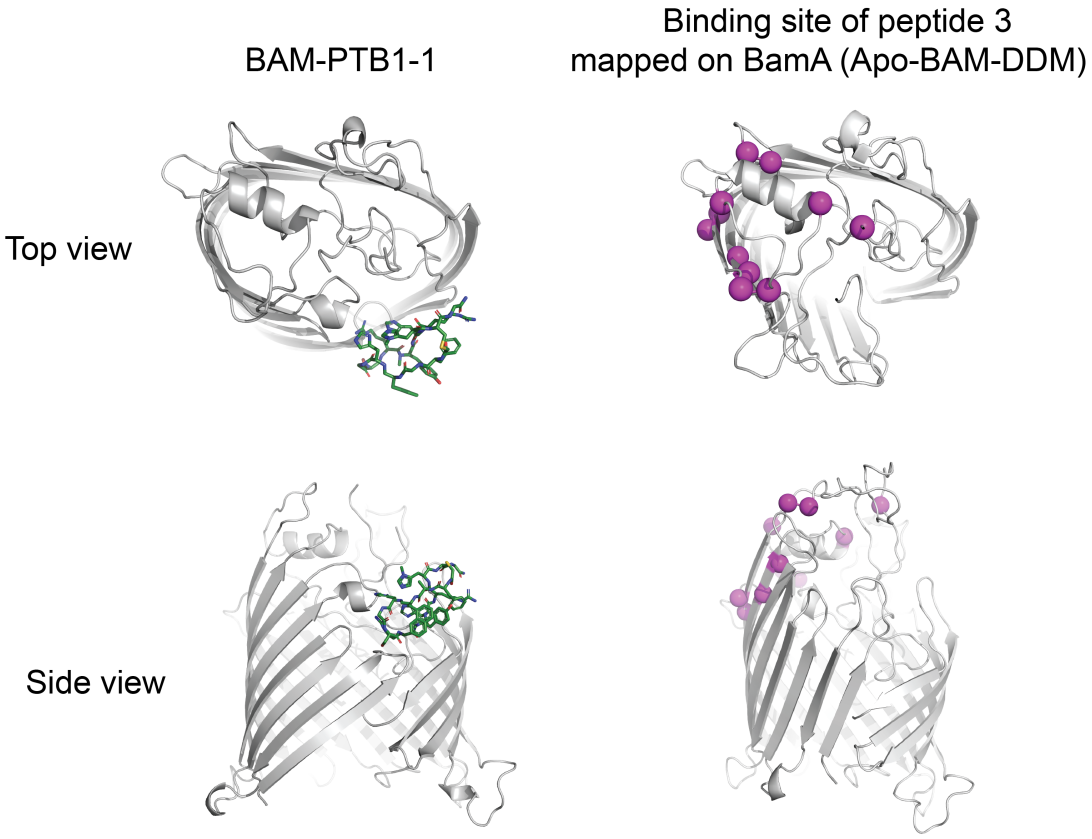

Supplementary Figure 14. Comparison of PTB1-1-BAM complex
Comparison of BamA β-barrel conformation in PTB1-1 bound state with BamA with the mapped peptide 3[3] binding site, which was mapped by solution NMR studies in[3] from both top view and side view. PTB1-1 is shown as a green stick model. The identified binding site of peptide 3 is indicated on the Apo-BAM-DDM structure as purple spheres.

Supplementary Table 1. Cryo-EM data collection, refinement, and validation statistics.

	PTB1-1-BAM **EMD-45765** **PDB 9CNX**	**Apo BAM-DDM** **EMD-45764** **PDB 9CNW**	**PTB2-BAM-DDM** **EMD-45767** **PDB 9CNZ**	**Apo BAM-SMA** **EMD-45766** **PDB 9CNY**	**PTB2-BAM-SMA** **EMD-45768** **PDB 9CO0**
Data Collection					
Magnification	165,000x	105,000x	130,000x	36,000x	165,000x
Voltage (kV)	300	300	300	200	300
Camera	Gatan K2 Summit	Gatan K3	Gatan K2 Summit	Gatan K2 Summit	Falcon 4i
Electron exposure (e/Å^2)	43	64	46	52	47
Defocus range (μm)	0.5–3.0	0.5–3.0	0.5–3.0	0.5–3.0	0.5–3.0
Pixel size (Å)	0.849	0.838	1.047	1.148	0.731
Energy filter slit width (eV)	20	20	20	—	20
Number of frames	80	60	50	60	40
Image Processing					
Symmetry imposed	C1	C1	C1	C1	C1
Particle box size (Å)	372	306	306	306	306
Number of micrographs (no.)	38,156	9,684	17,756	3,596	18,319
Final particle images (no.)	124,444	556,336	181,444	175,771	78,053
Map resolution (Å)	3.55	2.6	3.1	4.0	3.3
FSC threshold	0.143	0.143	0.143	0.143	0.143
Refinement					
Initial models used (PDB code)	PDB-5d0o	PDB-5ljo	PDB-5ljo	N/A Apo BAM-DDM	N/A PTB2-BAM-DDM
Volume CC	0.82	0.82	0.83	0.76	0.80
Ligand CC	0.78	—	0.66	—	0.60
Map-sharpening B-factors (Å^2)	-99	-111	-93	-169	-114
Non-hydrogen atoms	11582	11647	12854	10416	10766
Protein residues	1480	1493	1638	1333	1368
Waters	0	0	0	0	0
Ligands	2	0	3	0	3
R.m.s. deviations					
Bond lengths (Å)	0.003	0.004	0.004	0.004	0.003
Bond angles (°)	0.692	0.987	0.678	1.018	0.689
Validation					
MolProbity score	1.02	0.94	1.19	1.52	1.34
Clashscore	1.93	1.84	3.44	5.74	4.93
Poor rotamers (%)	0	0	0	0	0
Ramachandran Plot					
Favored (%)	97.73	98.24	97.77	96.66	97.62
Allowed (%)	2.27	1.76	2.23	3.34	2.38
Disallowed (%)	0	0	0	0	0

Supplementary Table 2. Crystallographic data collection and refinement statistics.

	PTB2-BamA PDB 9CO2
Data collection	
Space group	*P2₁*
Cell dimensions	
a, *b*, *c* (Å)	98.79, 167.27, 104.82
α, β, γ (°)	90, 110.99, 90
Resolution (Å)	97.86-2.74 (3.00-2.74)
Rpim	0.081 (0.485)
I / *sI*	6.0 (1.7)
Completeness (%)[a]	90.1 (53.1)
Redundancy	3.4 (3.4)
CC(1/2)	0.997 (0.774)
Refinement	
Resolution (Å)	29.59-2.75
No. reflections	47356 (281)
*R*work / R_{free}[b]	33.5/36.8
No. atoms[c]	12648
protein	12632
ligand	16
B-factors	60.40
protein	60.38
ligand	77.79
R.m.s. deviations	
Bond lengths (Å)	0.005
Bond angles (°)	0.90

Single crystal was collected for the data set.
Ramachandran plot: 94.85% favored, 4.64% allowed, 0.51% outlier.
[a] ellipsoidal completeness is 96.7% in 97.8-8.91 bin, but data were anisotropic in higher resolution shells (a*=4.29, b*=2.74, c*=2.78).
[b] 5% of reflections used to calculate R_{free}.
[c] represents all non-hydrogen atoms modeled.

Supplementary Table 3. Strains, plasmids, and primers used in this study.

IDENTIFIER	**DESCRIPTION**			
Strain number	**Species**	**Strain name**	**BamA mutation**	**Source**
GNE 115	*E. coli*	BW25113		[4]
GNE 178	*E. coli*	ATCC 25922		ATCC
GNE 15	*K. pneumoniae*	ATCC 43816		ATCC
GNE 18	*E. aerogenes*	ATCC 13048		ATCC
GNE 19	*E. cloacae*	ATCC 222		ATCC
GNE 23	*S. aureus*	USA300		
GNE 4349	*E. coli*	BW25113	N492K	in-house
GNE 4443	*E. coli*	BW25114	G437C	in-house
GNE 4458	*E. coli*	BW25115	G437S	in-house
GNE 4455	*E. coli*	BW25116	D464A	in-house
GNE 4460	*E. coli*	BW25117	D464N	in-house
GNE 4461	*E. coli*	BW25118	F492V	in-house
GNE 4462	*E. coli*	BW25119	Δ492-496insS	in-house
GNE 4455	*E. coli*	BW25119	F494A	in-house
GNE 4448	*E. coli*	BW25119	F494V	in-house
GNE 4449	*E. coli*	BW25120	A499V	in-house
GNE 4444	*E. coli*	BW25121	D500N	in-house
GNE 4452	*E. coli*	BW25122	L501P	in-house
GNE 4463	*E. coli*	BW25125	Q664H	in-house
GNE 4464	*E. coli*	BW25127	E800K	in-house

Sequencing primers	
bamA outside F	GCATCTGCTGTTCCTTGCGATC
bamA outside R	CGTGTTAGAAACACCGGTTTTCTG

Supplementary References

1. Gu et al. Structural basis of outer membrane protein insertion by the BAM complex. *Nature* **531**: 64-69 (2016).

2. Kaur et al. The antibiotic darobactin mimics β-strand to inhibit outer membrane insertase. *Nature* **593**: 125-129 (2021).

3. Luther et al. Chimeric peptidomimetic antibiotics against gram-negative bacteria. *Nature* **576**: 452-458 (2019).

4. Datsenko and Wanner. One-step inactivation of chromosomal genes in *Escherichia coli* K-12 using PCR products. Proceedings of the National Academy of Sciences **97**: 6640-6645 (2000).